EARTH SURFACE PROCESSES AND LANDFORMS
Earth Surf. Process. Landforms (2012)

Published online in Wiley Online Library
(wileyonlinelibrary.com) DOI: 10.1002/esp.3205

Hillslope response to tectonic forcing in threshold landscapes

Roman A. DiBiase,[1,2]* Arjun M. Heimsath[1] and Kelin X Whipple[1]
[1] School of Earth and Space Exploration, Arizona State University, Tempe, AZ USA
[2] Division of Geological and Planetary Sciences, California Institute of Technology, Pasadena, CA USA

Received 17 August 2011; Revised 4 January 2012; Accepted 9 January 2012

*Correspondence to: Roman A. DiBiase, Division of Geological and Planetary Sciences, California Institute of Technology, Pasadena, CA 91125, USA. E-mail: rdibiase@caltech.edu

ESPL
Earth Surface Processes and Landforms

ABSTRACT: Hillslopes are thought to poorly record tectonic signals in threshold landscapes. Numerous previous studies of steep landscapes suggest that large changes in long-term erosion rate lead to little change in mean hillslope angle, measured at coarse resolution. New LiDAR-derived topography data enables a finer examination of threshold hillslopes. Here we quantify hillslope response to tectonic forcing in a threshold landscape. To do so, we use an extensive cosmogenic beryllium-10 (^{10}Be)-based dataset of catchment-averaged erosion rates combined with a 500 km^2 LiDAR-derived 1 m digital elevation model to exploit a gradient of tectonic forcing and topographic relief in the San Gabriel Mountains, California. We also calibrate a new method of quantifying rock exposure from LiDAR-derived slope measurements using high-resolution panoramic photographs. Two distinct trends in hillslope behavior emerge: below catchment-mean slopes of 30°, modal slopes increase with mean slopes, slope distribution skewness decreases with increasing mean slope, and bedrock exposure is limited; above mean slopes of 30°, our rock exposure index increases strongly with mean slope, and the prevalence of angle-of-repose debris wedges keeps modal slopes near 37°, resulting in a positive relationship between slope distribution skewness and mean slope. We find that both mean slopes and rock exposure increase with erosion rate up to 1 mm/a, in contrast to previous work based on coarser topographic data. We also find that as erosion rates increase, the extent of the fluvial network decreases, while colluvial channels extend downstream, keeping the total drainage density similar across the range. Our results reveal important textural details lost in 10 or 30 m resolution digital elevation models of steep landscapes, and highlight the need for process-based studies of threshold hillslopes and colluvial channels. Copyright © 2012 John Wiley & Sons, Ltd.

KEYWORDS: threshold hillslopes; rock exposure; slope distributions; drainage density

Introduction

Steep, tectonically active landscapes provoke broad interest, both for geoscientists interested in interactions among climate, uplift, and erosion, and for an increasing global population that is encroaching deeper into landscapes exposed to landslides, floods, and earthquakes. Such regions are typically interpreted to be threshold landscapes – where rock strength limitations decouple mean hillslope angle from erosion rate, and prevent hillslopes from sustaining mean gradients steeper than 35 to 40° (Carson and Petley, 1970; Schmidt and Montgomery, 1995; Burbank *et al.*, 1996; Montgomery and Brandon, 2002). Mean slope is, therefore, a poor metric of landscape-averaged erosion rate in steep mountain ranges (Ouimet *et al.*, 2009; DiBiase *et al.*, 2010). However, even casual observation suggests that the fraction of exposed bedrock varies significantly in these 'threshold' landscapes and that local slopes can become extreme where rock is outcropping. The fact that much of the work pertaining to threshold hillslope morphology has been based on either detailed but spatially limited field measurements (e.g. Strahler, 1950) or coarse resolution topographic analyses (local slopes measured over 30–300 m) using digital elevation models (DEMs) (Burbank *et al.*, 1996; Montgomery, 2001; Binnie *et al.*, 2007; Korup, 2008; DiBiase *et al.*, 2010) raises the question of whether the observed constancy of mean slope is either an artifact of data resolution or the scale of analysis. Moreover, little is known about how hillslope form, texture, and length vary with erosion rate in steep landscapes. Key first-order questions remain unanswered for steep landscapes: How does rock exposure vary with erosion rate? How does the distribution of local slopes reflect changes in rock exposure? Does the length (and thus relief) of threshold hillslopes vary as a function of erosion rate? In short, do hillslopes in 'threshold' landscapes in fact record tectonic information?

The availability of high-resolution DEMs derived from airborne LiDAR surveys enables a detailed examination of the response of steep landscapes to tectonically driven erosion rate at the process (and outcrop) scale. The transformative potential of this increase in data resolution from ~30 m to ~1 m has been well appreciated by geomorphologists working in soil-mantled

landscapes (e.g. National Research Council, 2010). For example, Roering (2008) used high-resolution topography to discriminate among hillslope soil transport laws whose differences in topographic expression cannot be captured by coarser elevation data. Similarly, Hilley and Arrowsmith (2008) used a 1 m LiDAR DEM to quantify hillslope and channel response to time-varying rock uplift in weak sedimentary rocks along the San Andreas Fault, highlighting the potential to extract tectonic information from erosional landscapes given sufficiently detailed topographic data. We collected ~500 km^2 of high-resolution LiDAR topographic data in the San Gabriel Mountains, California (SGM) spanning a great diversity in landscape form and surface character in order to study the behavior of threshold landscapes in more detail than previously possible.

Here we quantify hillslope response to tectonics across a threshold landscape using this 1 m resolution, LiDAR-derived DEM, high resolution (<0·1 m) panoramic photographs, and cosmogenic beryllium-10 (^{10}Be)-derived catchment averaged erosion rates. We build on extensive previous work to investigate how hillslope bedrock exposure, slope angle distribution, and drainage density vary across a gradient in relief and erosion rate in the SGM that is expressed as a transition from soil mantled to increasingly rocky hillslopes. We describe and calibrate a new method of quantifying rock exposure using high resolution slope measurements; we calculate statistics from hillslope gradient distributions at a range of spatial scales; and we use small (2–3 km^2), representative catchments to evaluate how hillslope length varies in this landscape through an analysis of drainage density variations.

Study Area: Setting, Erosion Rates, and Analysis Strategy

The SGM present an excellent landscape for studying the transition from soil-mantled to rocky hillslopes. A large restraining bend in the San Andreas Fault produces a strong west–east gradient in uplift rate, erosion rate, and topographic relief, whereas climate (mean annual precipitation ~0·7–1·0 m) and lithology (predominately granitic rocks) do not vary much across the 100 km wide range (Peterson and Wesnousky, 1994; Spotila *et al.*, 2002; Lavé and Burbank, 2004; DiBiase *et al.*, 2010). DiBiase *et al.* (2010) exploited this gradient in tectonic forcing to quantify the topographic controls on erosion rates determined from detrital cosmogenic ^{10}Be concentrations and provide a more detailed description of the field area and tectonic setting. Catchment erosion rates averaged over millennial timescales range from 35 to 1100 m/Ma, and correlate with catchment-mean hillslope angle for slopes less than 30° and erosion rates less than ~300 m/Ma. For steeper slopes and more rapid erosion rates, mean hillslope angle [as measured on 30-m and 10-m US Geological Survey (USGS) DEMs] in catchments 1–150 km^2 in size appears to become decoupled from erosion rate, similar to findings in previous studies of other steep landscapes (Montgomery and Brandon, 2002; Binnie *et al.*, 2007; Ouimet *et al.*, 2009; Stock *et al.*, 2009; Norton *et al.*, 2010). This transition from slope-dependent to effectively slope-independent erosion rates agrees with predictions from nonlinear soil transport models (Roering *et al.*, 1999; Roering *et al.*, 2007), and corresponds with the onset of mass wasting and rock exposure on hillslopes in this landscape (Heimsath *et al.*, 2012). However, in contrast to predictions of most hillslope evolution models (e.g. Tucker and Hancock, 2010; and references cited therein), the transition to threshold hillslopes does not result in an abrupt loss of the soil mantle; rather, rock exposure remains patchy and significant soil cover persists throughout the range. What controls the extent of rock exposure and how does this affect the distribution of local slopes? Heimsath *et al.* (2012) showed that soil production rates increase with catchment-averaged erosion rates in the SGM, even in regions where stochastic landslides create a patchwork of rock and soil cover on hillslopes. This increase in soil production rates, coupled with the fact that landsliding spatially concentrates erosion, explains the persistence of significant soil cover at high erosion rates (Heimsath *et al.*, 2012). We extend this work by developing a robust metric of rock exposure and performing a systematic analysis of the response of hillslope morphology to differences in erosion rate.

An important aspect of our study is the spatial correspondence of a 500 km^2 LiDAR-derived 1 m resolution DEM with an extensive soil production and catchment-averaged erosion rate data set quantified from cosmogenic ^{10}Be concentrations in quartz from saprolite and alluvial sands (DiBiase *et al.*, 2010; Heimsath *et al.*, 2012). We supplement this dataset with eight additional alluvial sand samples draining catchments ranging from 2 to 26 km^2 (Table I).These eight samples were collected and processed using the methods detailed in DiBiase *et al.* (2010). To determine erosion rates, we implemented a pixel-by-pixel calculation of elevation and latitude production rates caling factors calibrated by Dunai (2000), using a density of 2·6 g/cm^3 and a sea level, high latitude production rate of 5·1 atoms/g/yr.

To focus our DEM-based topographic analyses further we selected a set of 20 small catchments, averaging 2–3 km^2 in size (Table II). These catchments lie within both the coverage of our catchment-averaged erosion rates and of the high-resolution LiDAR DEM, are spatially homogeneous (i.e. no major knickpoints or large landslides), and span a wide range of hillslope texture, from low relief and soil mantled to steep and rocky. Many of these catchments coincide directly with detrital cosmogenic ^{10}Be sample locations. For catchments with multiple or nested cosmogenic ^{10}Be rates, we used the nearest sample, or averaged the

Table I. Catchment averaged erosion rates from cosmogenic ^{10}Be concentrations

Sample ID	Easting[a]	Northing[a]	Area (km^2)	^{10}Be/SiO$_2$ ($\times 10^3$ atoms/g)	N(z,I)[b]	Erosion rate (m/Ma)[c]
SG160	429950	3795861	18·8	14·82 ± 2·44	4·16	907 ± 195
SG0706	398469	3783358	17·3	10·79 ± 1·91	2·02	605 ± 137
SG0708	399180	3794240	1·9	18·89 ± 1·99	2·54	435 ± 68
SG0747	406053	3786078	7·3	11·81 ± 3·51	1·97	541 ± 188
SG0748	406129	3785893	7·4	11·77 ± 2·61	1·97	541 ± 147
SG0749	406010	3784661	6·1	10·53 ± 2·83	1·99	611 ± 195
SG0818	391759	3790469	25·5	9·98 ± 1·33	2·19	711 ± 130

[a]UTM coordinates (NAD 27 Datum).
[b]Production rate latitude/elevation scaling factor (Dunai, 2000).
[c]Erosion rates calculated using density of 2·6 g/cm^3, attenuation length of 165 g/cm^2, and high latitude production rate of 5·1 atoms/g/yr.

Table II. Study catchment characteristics

ID	Name	Area (km^2)	Cosmogenic ^{10}Be sample	E (m/Ma)	S_{mean}	σ_S	S_{mode}	Skewness (S)	REI	$S_{colluvial}$	Total D_d	Fluvial D_d	Colluvial D_d
1	Chilao	2·3	SG128[a]	42 ± 6	16·2	7·5	15·0	0·47	0·1	14·6	11·8	10·5	1·3
2	Big Rock 1	3·8	SG0809[b]	434 ± 59	35·7	8·9	36·8	−0·38	8·2	32·7	8·4	3·5	4·9
3	Big Rock 2	2·5	SG0804[b]	493 ± 111	33·8	9·7	36·4	−0·80	6·8	—	—	—	—
4	Mule Fork	3·8	SGB2[a], SG124[a]	150 ± 50[c]	28·1	9·4	32·2	−1·31	1·7	24·5	11·0	7·9	3·1
5	Little Bear	2·0	SG0818	711 ± 130	36·9	10·1	37·4	−0·13	12·4	—	—	—	—
6	Lucas	2·3	SGB7[a]	253 ± 54	37·5	8·7	38·2	−0·24	11·6	—	—	—	—
7	Millard	2·1	SG0704	668 ± 186	36·1	9·6	37·4	−0·41	10·0	—	—	—	—
8	Santa Anita	2·0	SG0748	541 ± 147	38·0	9·8	39·8	−0·54	16·7	33·1	9·9	5·6	4·3
9	Winter	2·6	SG0749	611 ± 195	39·8	10·3	39·4	0·12	21·3	35·1	9·6	2·7	6·9
10	Upper Eaton	2·3	SG127[a]	736 ± 99	42·0	11·1	38·2	1·01	26·1	36·1	10·1	2·9	7·2
11	Deer Branch	2·3	SG126[a]	591 ± 71	39·6	10·1	39·6	−0·01	20·7	—	—	—	—
12	Harvard Branch	2·0	SG125[a]	465 ± 61	37·8	10·3	38·6	−0·23	16·8	—	—	—	—
13	Upper SF Iron	2·0	SG151[a], SG152[a]	256 ± 180	31·8	8·0	35·2	−1·29	2·5	—	—	—	—
14	North Iron Fork	2·5	SG160	907 ± 195	41·8	10·6	38·0	1·08	24·9	—	—	—	—
15	South Iron Fork	2·1	SG161[a]	1006 ± 191	42·7	10·5	38·4	1·21	28·6	35·5	10·5	3·2	7·3
16	Big Rock 3	3·2	SG0805[b]	343 ± 58	33·0	9·2	35·6	−0·84	5·0	29·8	7·8	3·6	4·2
17	Little Rock 1	2·6	SG131[a]	98 ± 17	20·2	7·7	20·6	−0·15	0·1	18·0	12·2	10·7	1·5
18	Little Rock 2	1·2	SG132[a]	106 ± 10	22·2	7·9	25·0	−1·07	0·1	—	—	—	—
19	Clear	3·0	SGB10[a]	279 ± 23	32·4	12·0	36·2	−0·96	8·3	—	—	—	—
20	Wickiup	1·9	SG0708	435 ± 68	35·6	7·5	37·8	−0·87	4·8	—	—	—	—

Source for cosmogenic ^{10}Be data:
[a]DiBiase *et al.*, 2010;
[b]Heimsath *et al.*, 2012.
[c]Poor cosmogenic ^{10}Be coverage.
Note: slope measurements are in degrees, drainage density measurements are in units of 1/km.

erosion rate as indicated in Table II. We combined field mapping with topographic analyses and this database of catchment-average erosion rates to determine (1) a robust topographic metric for the spatial extent of rock outcrop, (2) how rock exposure varies with erosion rate, (3) how the change in process from soil creep to rapid mass wasting and progressive exposure of rock outcrops affect the distribution of local slope angles, (4) how hillslope length (or drainage density) varies with erosion rate, and (5) how the drainage network is partitioned between fluvial channels and colluvial headwater channels as defined below.

Analysis of variations in hillslope length, or drainage density, with erosion rate is complicated by the partitioning of the valley network into 'colluvial' channels in the catchment headwaters and 'fluvial' channels downstream. It is important to recognize that the colluvial–fluvial transition is distinct from the hillslope–channel transition (Montgomery and Foufoula-Georgiou, 1993). Channel profiles in the SGM (and elsewhere) exhibit an abrupt break in morphology from a headwater segment where slope is independent of drainage area to a downstream segment well described by Flint's law, where slope decreases as a power law with drainage area (see Supporting Information). This break in slope-area scaling has been interpreted to indicate a handover in process dominance from debris flow to fluvial incision (Montgomery and Foufoula-Georgiou, 1993). Although Stock and Dietrich (2003) have argued that this transition is more gradual, we follow Montgomery and Foufoula-Georgiou (1993) in defining the 'colluvial'–'fluvial' transition as the center point of this change in slope-area scaling. As such, the terms 'colluvial' and 'fluvial' refer to slope-area scaling properties, and not necessarily a discrete change in process dominance; debris flows are known to runout beyond this morphological transition in the SGM (and elsewhere) and presumably contribute to channel incision processes, and thus influence channel slope (Stock and Dietrich, 2003, 2006). Nevertheless, as illustrated in the Supporting Information, it is this break in slope-area scaling that defines a significant change in landform response to tectonically-driven erosion rate. We do not address the role of debris flows in channel incision as a function of drainage area, but rather restrict our focus to the relation between the average slope of 'colluvial' channels upstream of this readily identified break in slope-area scaling, and how it relates to hillslope gradient and relief.

Rock Exposure

Steep hillslopes in the SGM and elsewhere are typically composed of a patchwork of colluvial soil, scree, and exposed rock. Soils tend to be coarse, thin (<20 cm), and lack distinct horizons. Extensive observations of the soils across the field area confirm that they are similar to soils studied on other hilly and mountainous landscapes and are well described by the conceptual framework developed for such soils (e.g. Heimsath *et al.*, 1997; Heimsath *et al.*, 2005). In this framework, colluvial soils can include rockfall sources, but are dominated by clasts physically disrupted from the underlying parent material and then transported downslope within the soil. The emergence of bedrock outcrops signals that erosion locally exceeds soil production and supply, potentially indicating a change in erosion process from steady to stochastic. To quantify how the spatial extent of rock exposure changes with erosion rate we focus our mapping efforts on the hillslope distribution of in-place and exposed bedrock (as opposed to transportable rock debris). These exposures tend to be blocky, fractured masses that range in scale from 0·1 to 100 m, but planar bedrock flush with the soil surface is not uncommon. Near vertical cliff faces greater than 10 m are rare.

To quantify how bedrock exposure varies with erosion rate, we selected 11 hillslopes that range in scale from 0·1 to 1 km^2, have minimal vegetation (as a result of recent fires, for example), and that span a wide range of rockiness. For each hillslope, we used unobstructed, approximately surface-normal views to construct large panoramic images (up to 3×10^8 pixels) with 1–10 cm spatial resolution. Using these panoramas, we selected eight 100 m × 100 m patches for detailed mapping of bedrock exposure (Figure 1), with the remainder of the imagery used for spot checking our rock exposure metric defined later. These small patches were chosen to span a wide range

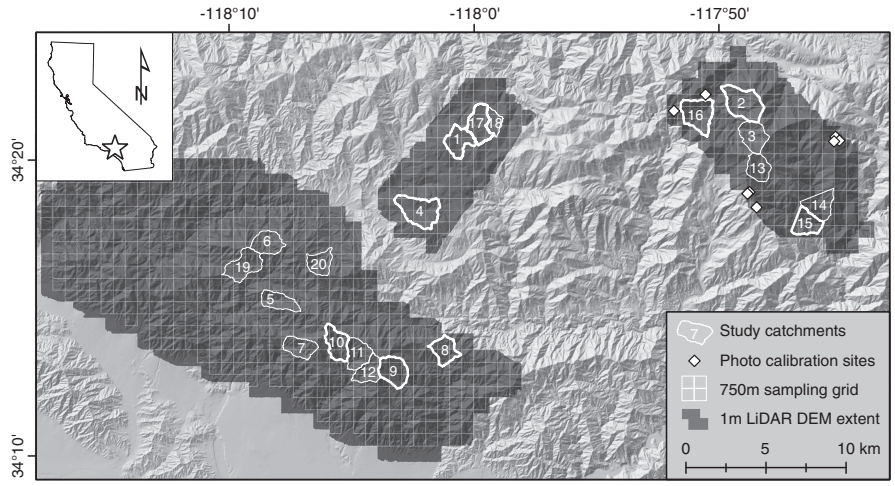

Figure 1. Shaded relief map of San Gabriel Mountains, California (SGM). Outlines of study catchments are shown as white lines, with labels corresponding to Table II. Bold outlines indicate catchments used for drainage density analysis (Figure 8). White diamonds indicate sites where panoramic photographs were used to calibrate the Rock Exposure Index (REI). White grid highlights the block sampling scheme used for topographic analysis across the extent of the 1 m LiDAR DEM (dark gray).

of surface texture, from mostly soil mantled with occasional tors, to steep, rocky cliff faces and debris chutes. We chose a spatial scale of 100 m to ensure our mapping area was larger than the typical outcrop size (order 10 m), but small enough to allow for detailed and efficient mapping over a range of hillslopes. We mapped directly on the photographs, and projected the bedrock polygons to plan-view maps using perspective hillshade surfaces from the 1 m LiDAR DEM (Figure 2, Supporting Information). We define measured bedrock exposure as the plan-view ratio of mapped bedrock to total area.

We calibrated our maps of rock exposure to a metric based on local slope, measured as the dip of a 3 m × 3 m plane fitted at each point on the 1 m LiDAR DEM. We define this new metric, the Rock Exposure Index (REI), as the percentage of cells within a given area greater than a critical slope, S_*, multiplied by a correction factor (of order one) such that REI is a direct proxy for percent bedrock exposure. For each of our eight calibration patches, we calculated REI for S_* equal to 40°, 45°, and 50° (Figure 3). Measured bedrock exposure increases monotonically with REI for each value of S_*, though the strongest linear correlation is with a critical slope of 45° ($R^2 = 0{\cdot}99$). Field observations elucidate why $S_* = 45°$ is most effective in this landscape; soil-mantled slopes between 40° and 45° exist but are uncommon and we have not found soil-covered slopes or scree slopes in the SGM with slopes steeper than 45°. However, bedrock outcrops gentler than 45° do occur, and likely contribute to the deviation of the regressed slope from 1:1 (Figure 3), but are uncommon. Field reconnaissance with classified slope maps reveals that nearly all in-place bedrock exposed on hillslopes in the SGM is captured by our metric, and that false positives are minimal – a finding corroborated by the detailed analysis of high resolution panoramic photographs as described above. The robust linear correlation in Figure 3 and our extensive field observations give us confidence that REI provides an effective measure of percent rock exposure in the SGM over spatial scales greater than 100 m.

Slope Distributions

To compare hillslope morphology at the catchment scale, we used the 20 small catchments that span a range of morphology from low gradient, smooth and soil mantled to steep, rocky and rugged terrain (Figure 1, Table II). For each catchment, we generated a slope map from the 1 m LiDAR DEM, and extracted slope histograms normalized by the area analyzed (subset shown in Figure 4a). For comparison, we extracted the same information using the freely available 10 m USGS NED DEM (Figure 4b). While the catchment-mean slopes from both datasets are tightly correlated, Figure 4 highlights the inadequacies of the USGS data to accurately capture the details of hillslope distributions. Using the 1 m LiDAR DEM, we determined the mean (S_{mean}), mode (S_{mode}), standard deviation (σ_S), and skewness for each slope distribution, and used the REI described earlier to estimate the percentage of outcropping rock for each basin (red filled circles, Figure 5). Because S_{mode} is sensitive to binning choice, we visually inspected histograms with a range of bin sizes to choose the smallest bin size that retains a smooth histogram (0·1°, Figure 4).We used the Pearson skewness coefficient, defined as skewness $= 3 \times (S_{mean} - S_{mode})/\sigma_S$. We find that for catchments with S_{mean} less than ~30°, little to no rock is exposed, modal slopes increase with mean slopes, and the skewness of the slope distribution decreases with increasing mean slope. For catchments with S_{mean} greater than 30°, rock exposure and skewness increase strongly with mean slope, while modal slopes increase only slightly, and stay similar to values of angle-of-repose debris slopes observed in the field (36°–38°). The standard deviation of the slope distribution is weakly correlated with mean slope (Table II, $R^2 = 0{\cdot}45$).

Plotting mean slope against erosion rate reveals a similar relationship to that quantified by DiBiase *et al*. (2010), although mean slopes do not become invariant above 300 m/Ma but rather continue to increase slowly with erosion rate (Figure 6a). This is likely due primarily to choosing small, representative basins rather than whole catchments varying widely in scale (up to 150 km^2) as done in our earlier work (DiBiase *et al.*, 2010). As discussed below, the higher resolution of the LiDAR DEM used here does not much affect estimates of mean slope. While mean slope increases slowly with erosion rate for steep catchments, rock exposure as measured by REI increases approximately linearly with erosion rate for steep ($S_{mean} > 30°$) catchments in the SGM, but with considerable scatter (Figure 6b). Slowly eroding catchments (<150 m/Ma) are nearly entirely soil mantled (REI < 0·1). The relationship shown in Figure 6b is consistent with predictions from a simple landslide model (Heimsath *et al.*, 2012) and observations by Norton *et al*. (2010).

We extended the earlier analysis to the entire landscape within the LiDAR coverage by breaking up the landscape into a 750 m × 750 m square grid (Figure 1) and computing the same slope statistics for each block, similar to the

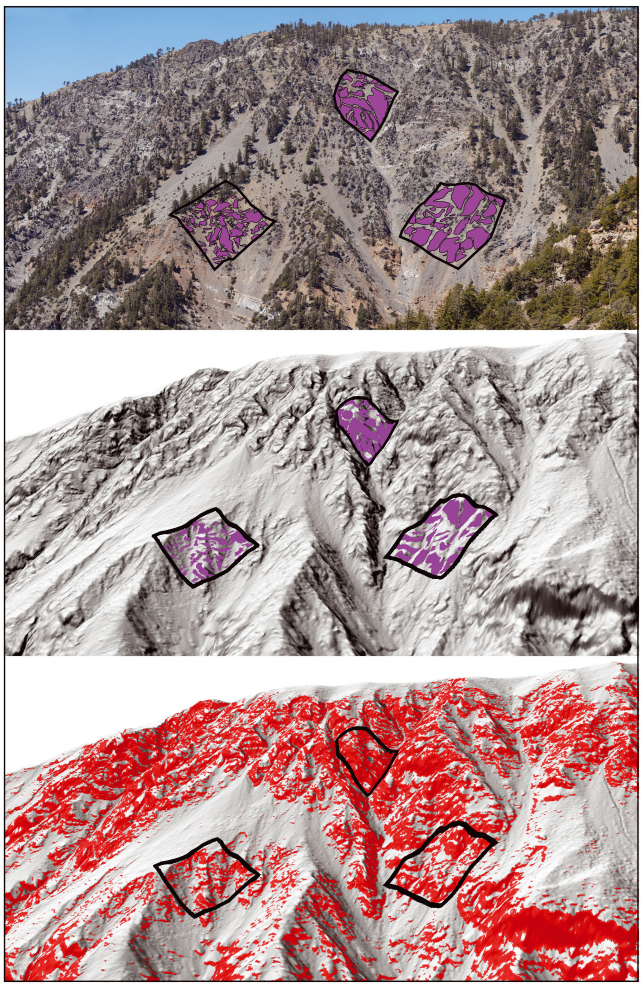

Figure 2. Example of rock exposure calibration from east slope of Mount Baden-Powell. Top panel shows high-resolution (1 cm) photograph overlain by three mapping patches (black outlines, 1 ha each). Purple polygons indicate mapped rock exposure, which is transferred to plan-view maps using shaded relief images tilted to the same perspective as the photograph (middle panel). The bottom panel highlights pixels with slope greater than 45° (red).

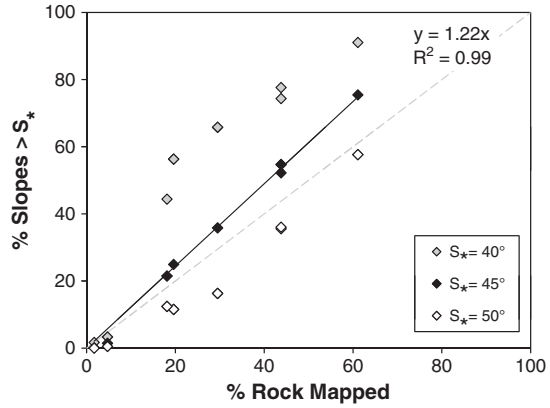

Figure 3. Plot of percentage of slopes greater than S_* against percent rock mapped from panoramic photographs. The best linear fit is for $S_* = 45°$, and we use this calibration to define our Rock Exposure Index (REI). Dashed line indicates 1:1 relationship.

methodology used by Montgomery (2001), Wolinsky and Pratson (2005), and Korup (2008) for their coarser scale DEM analyses. We chose a scale of 750 m to mimic the lower end of existing detrital erosion rate catchments (DiBiase *et al.*, 2010), capture full crest-swale hillslopes,

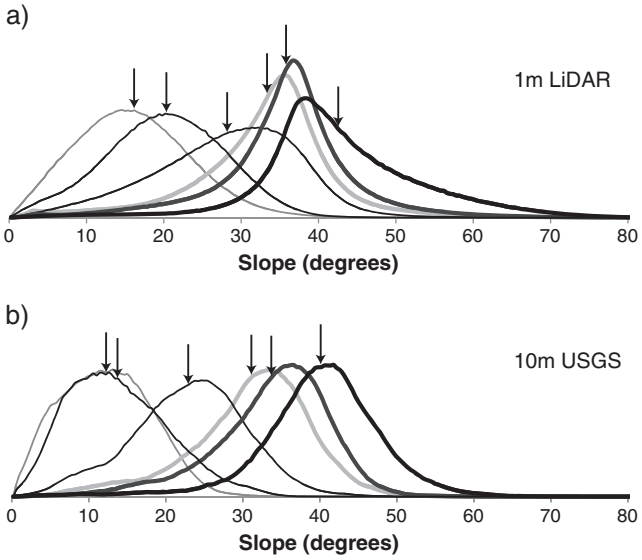

Figure 4. Slope histograms generated from sample catchments using the 1 m LiDAR DEM (a) and the 10 m USGS DEM (b). Arrows indicate the mean slope for each of the catchments used (from left to right: basin 1, 17, 4, 16, 2, 15). While the mean slope generated from the two datasets is correlated, there are significant differences in histogram shape, including the sign of the skewness for steep catchments.

and yet reveal patterns and variations in landscape texture. Results from this analysis corroborate results from the 2–3 km^2 catchments, demonstrating that these catchments are indeed representative of landscape morphology within the SGM (gray crosses, Figure 5).

Hillslope Length and Drainage Density

For nine of the 20 small catchments, we extracted the total valley network, identified the transition from colluvial to fluvial slope-area scaling, and calculated the colluvial, fluvial, and total drainage density. Despite progress (Stock and Dietrich, 2003, 2006), the extent of the channel network importantly influenced by debris flow processes is not easily determined. Determining the extent of 'colluvial' and 'fluvial' channels as defined above, however, is readily done and illustrated below. Objectively defining the total channel drainage density (and thus hillslope length), especially across varied terrain, remains a fundamental challenge in geomorphology. In low-relief, soil-mantled landscapes, slope-area and local curvature metrics have been shown to be effective at defining channel heads and thus total drainage density (e.g. Montgomery and Dietrich, 1988, 1989; Tarboton *et al.*, 1992; Montgomery and Foufoula-Georgiou, 1993). However, as first pointed out by Montgomery and Foufoula-Georgiou (1993), headwater channels in steep terrain (so called 'colluvial' channels) are not readily distinguished from steep threshold hillslopes on the basis of slope-area data. Evaluating the relation between total drainage density and erosion rate in the SGM requires a method that will work in both low-relief, soil-mantled landscapes and steep, rocky landscapes.

Although we have not solved this problem, we found that the most consistent method for mapping total drainage density in both soil-mantled and rocky landscapes involved identifying zones where contributing area increased rapidly, as occurs at channel heads and along channel banks and can be directly resolved in high-resolution LiDAR DEMs. We resampled the 1 m LiDAR DEM to 4 m, and smoothed the re-sampled DEM with a three cell radius moving average window to remove

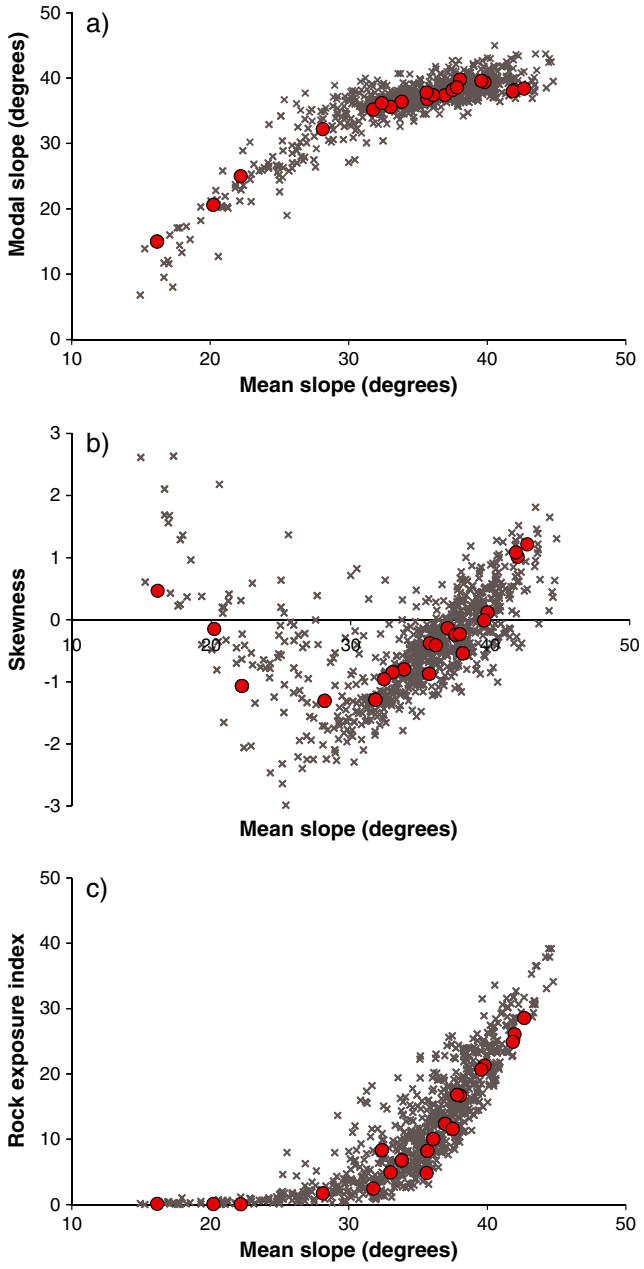

Figure 5. Slope statistics calculated using 2–3 km^2 sample catchments (red circles) and across 750 m × 750 m square grid (gray crosses). Plotted against mean slope are modal slope (a), skewness (b), and Rock Exposure Index (REI) (c). Note the inflection at mean slopes of 30° present in all three plots, highlighting the onset of significant rock exposure and the prevalence of angle-of-repose debris wedges that hold modal slopes near 37°. This figure is available in colour online at wileyonlinelibrary.com/journal/espl.

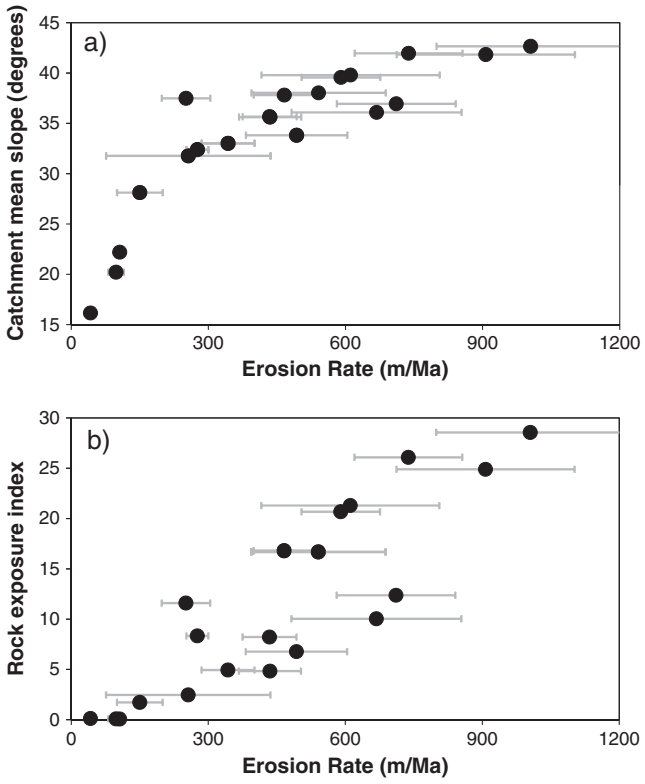

Figure 6. Plot of mean slope from 1 m LiDAR (a) and Rock Exposure Index (REI) (b) against detrital cosmogenic ^{10}Be erosion rate for the 20 study catchments listed in Table II.

high-resolution topographic noise that tends to reflect transient processes (e.g. recent tree throw pits). Such smoothing is often necessary for topographic analysis using LiDAR data (e.g. Roering, 2008). From the smoothed LiDAR DEM, we generated a grid of total contributing area from the D_{inf} flow direction model using the software package TauDEM (Tarboton, 1997). We then made a gradient map of the log of contributing area grid to highlight zones of rapid convergence. Using this map draped over the LiDAR shaded relief image, we hand-selected channel heads using pixels where the logarithm of contributing area increases by 10% or greater (Figure 7, top). This resulted in 100–150 channel heads for each of the nine catchments. We defined the channel network as the downstream extent of drainage network below these channel heads. While this methodology is subjective, it agrees with qualitative assessments of landscape dissection (from shaded relief maps and field observation) better than a simple threshold area classification or curvature- and slope-area-based metrics that work in soil-mantled landscapes but not in steep landscapes dominated by planar hillslopes, rugged rock outcrops, and colluvial channels. Although close inspection of the resultant drainage networks suggests that our method somewhat underestimates total drainage density in steep landscapes, we argue that this method is sufficiently accurate for a first-order evaluation of the relation between hillslope length and erosion rate and of the relative extent of the colluvial and fluvial valley networks as a function of erosion rate. Nevertheless, our estimation of total drainage density carries the greatest uncertainty in our analyses. Recent work by Passalacqua *et al.* (2010a, 2010b) to develop a channel extraction algorithm based on non-linear smoothing methods and global 'geomorphic cost' analysis shows promise for automating drainage density calculations in varied landscapes. However, testing such methods is difficult in steep, rocky landscapes due to uncertainty in identifying channel heads that may be buried by scree and dry ravel more rapidly than hollows in soil mantled landscapes (e.g. Reneau *et al.*, 1990).

We used the hand-picked channel heads to extract channel long profiles from the 1 m LiDAR DEM at vertical intervals of 3 m using the freely available Profiler Toolbar for ArcMap and Matlab (http://www.geomorphtools.org) (see Wobus *et al.*, 2006). Log-log plots of downstream slope against contributing area show scaling relationships typically observed in mountainous landscapes (Figure 7, bottom) (see also Supporting Information). Colluvial channel tips tend to have uniform slopes (horizontal line in slope-area space), while reaches downstream of ~10^5 m^2 exhibit concave-up, Flint's law scaling consistent with expectations for fluvial channels (Whipple and Tucker, 1999; Wobus *et al.*, 2006). As mentioned earlier, this transition in channel profile shape (from constant slope to concave in profile) is often cited as the topographic signature of the transition from debris-flow or colluvial to fluvial channels

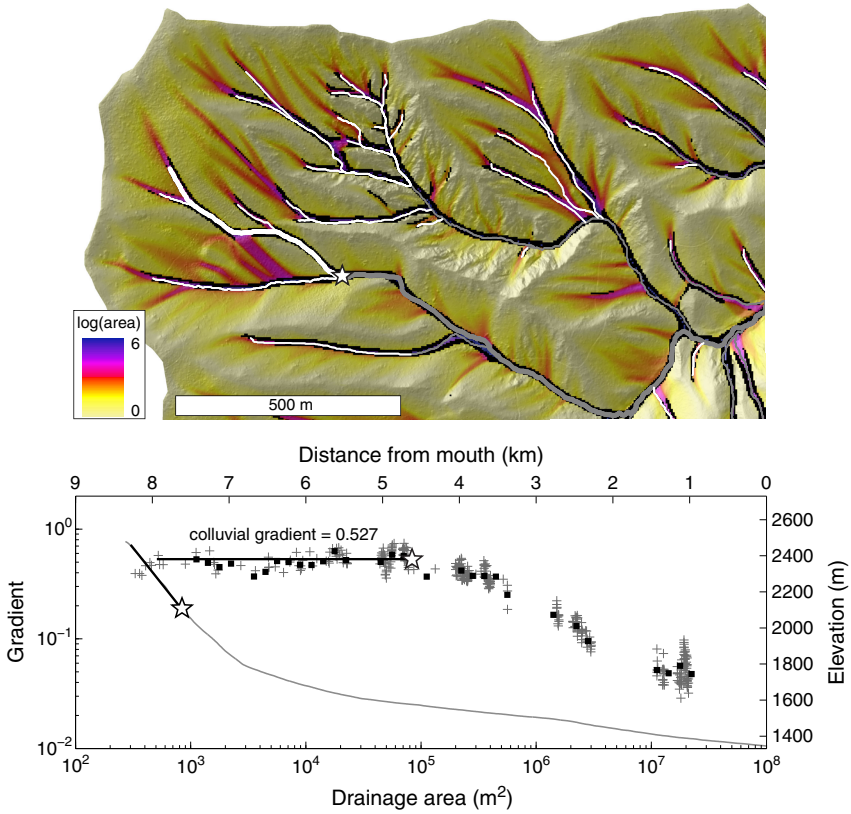

Figure 7. Channel network delineation for catchment 16 (Big Rock 3). D_{inf} contributing area shown over LiDAR shaded relief (top); black pixels highlight areas where contributing area increases rapidly (see text for details). White (colluvial) and gray (fluvial) lines show channel network resulting from hand-picked channel heads. Example slope-area plot and long profile (bottom) shown for bold channel, with star indicating transition from colluvial to fluvial scaling. Crosses indicate slope and area data from the 1 m DEM sampled at a 3 m contour interval, while squares indicate log-binned averages.

(Montgomery and Foufoula-Georgiou, 1993; Stock and Dietrich, 2003). We chose the center of this kink to define a discrete scaling transition, as it is easily identifiable in most SGM channels, particularly for short tributaries feeding into larger channels. Somewhat surprisingly, steep channels in the SGM often exhibit Flint's law scaling to slopes of 50% or greater (Figure 7, bottom) – regions typically interpreted to be heavily influenced by debris flows. We emphasize that our distinction between colluvial and fluvial channels is one based on a topographic scaling transition, rather than direct observation of process dominance. Notably, this break demarcates a dramatic change in landform response to erosion rate (see Supporting Information). For each hand-picked channel head, we identified this transition, and measured the average slope of each colluvial channel segment (Figure 7, bottom).

From this analysis, we quantified the following metrics for each catchment analyzed: total drainage density, defined as the total channel length divided by catchment area; fluvial drainage density, defined by the extent of the fluvial slope-area scaling; colluvial drainage density, equal to total minus fluvial drainage density; and mean colluvial slope, defined as the average slope of all colluvial channel segments weighted by length (Figure 8, Table II). As noted earlier, because of uncertainties in defining the upper extent of the channel network in steep landscapes, total drainage density and thus colluvial drainage density is likely underestimated slightly.

We find that fluvial drainage density decreases with increasing erosion rate (Figure 9a). This observation is consistent with predictions by Howard (1997) and Tucker and Bras (1998) for threshold landscapes where slopes lengthen with increasing relief because whereas channels steepen with increasing erosion rate, threshold hillslopes do not, resulting in a downstream shift in the position where channels reach the threshold slope. In the SGM, this decrease in fluvial drainage density, however, is offset by an increase in colluvial drainage density, such that the total valley density stays similar across the landscape (Figures 9b and 9c). Thus hillslope length, and therefore relief, varies little with erosion rate, and it is colluvial channels, and not hillslopes, that extend downstream as the landscape responds to an increase in erosion rate. The dissection of the long, planar hilllslopes predicted by simple landscape evolution models (e.g. Howard, 1997; Tucker and Bras, 1998) and the extension of the colluvial channel network is the most dramatic impact of debris flows on landscape form. Although the total drainage density depends directly on our uncertain identification of channel-heads, we argue that our interpretation of colluvial channels growing downstream at the expense of the fluvial network is robust – the colluvial–fluvial transition point clearly moves downstream as erosion rate increases (Figure 8; Supporting Information).

Interestingly, the mean slope of colluvial channels is tightly correlated to, and slightly lower than, the mean catchment slope (Figure 10). Whether this is a signature of debris flow processes responding to increased base level fall, or simply a geometric necessity for convergent topography (e.g. Schorghofer and Rothman, 2002) remains unclear. Either way, our data suggest that the controls on colluvial channel slope are not much different from the controls on mean hillslope angles – an observation that merits further research. Combined with the increase of colluvial drainage density, the increase of colluvial channel slopes with catchment averaged erosion rate implies an increase of colluvial relief with erosion rate. Consequently, the change in fluvial relief with erosion rate depends primarily on the scale of analysis: whereas fluvial relief increases with erosion rate in large catchments (e.g. DiBiase *et al.*, 2010), in small

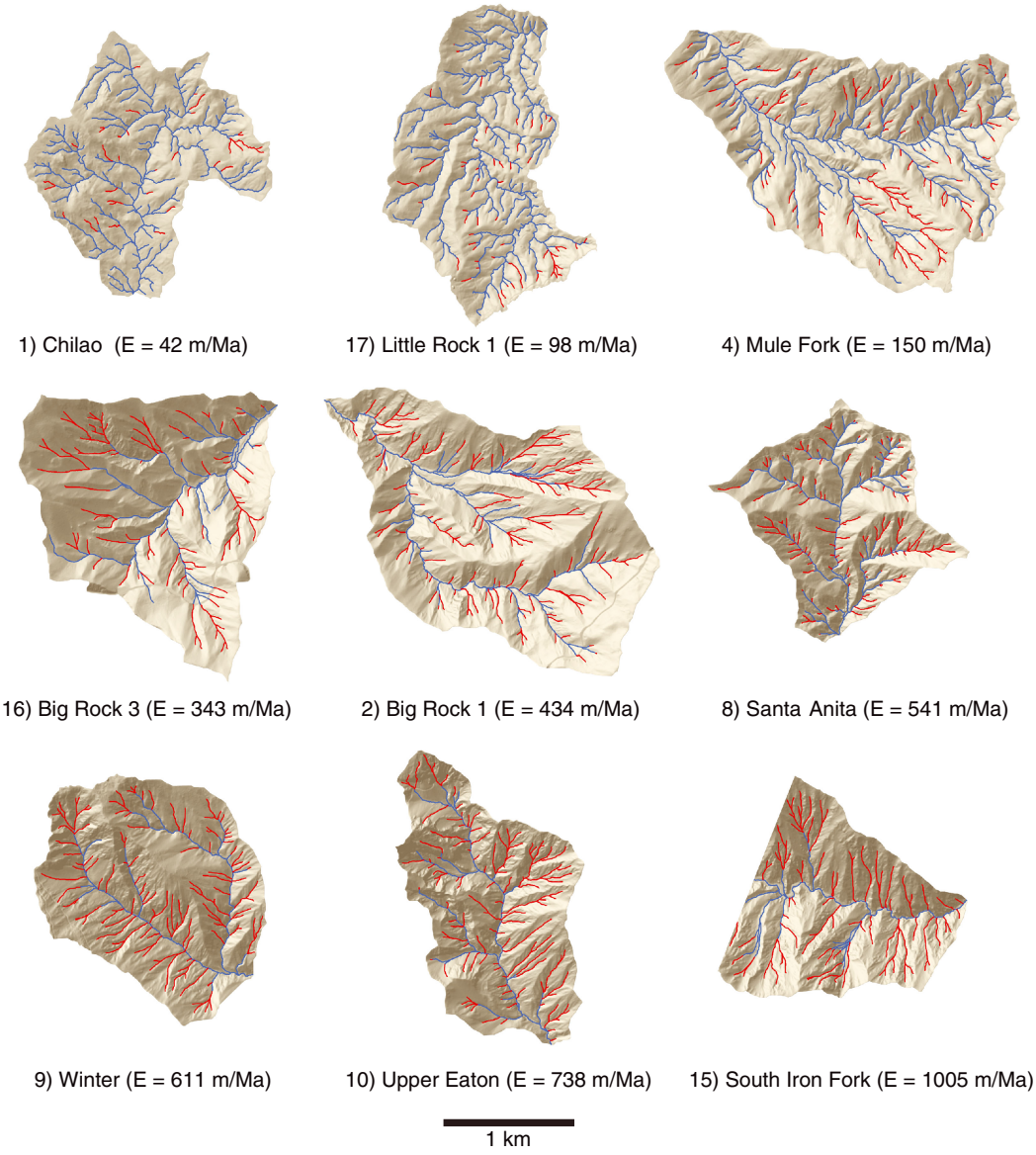

Figure 8. Shaded relief maps of nine study catchments used for drainage density analysis. Blue lines indicate channel network with fluvial slope-area scaling and red lines indicate colluvial channels. As erosion rates increase, colluvial drainage density increases at the expense of the fluvial network, while total drainage density remains roughly steady.

catchments fluvial relief actually decreases with increasing erosion rate due to the expansion of the colluvial channel network.

Discussion

LiDAR-derived slope distributions in the SGM vary systematically with mean slope, with notable changes in distribution shape occurring precisely at the point where we begin to see outcropping rock (mean slope ~30°, Figure 5c). Below mean slopes of 28°, skewness and mean slope are inversely correlated, similar to findings by Wolinsky and Pratson (2005). For mean slopes greater than 30°, modal slope becomes decoupled from mean slope and hovers between 36° and 38° (Figure 5b), which results in a strong positive relationship between skewness and mean slope. Wolinsky and Pratson (2005) used a simplified two-dimensional (2D) landscape evolution model to argue that the transition from creep- to failure- dominated catchments is characterized by a decrease in skewness. Our data supports this interesting finding for soil-mantled landscapes with mean slopes less than 30°. Additionally, they found a weak positive relationship between skewness and S_{mean} at high mean slopes, which they attributed to glacial processes. While this may be a signature of glaciated terrain, the inflection point in Figure 5 is due not to glacial processes, which are absent in the SGM. Rather, we interpret this inflection as response to an increase in bedrock exposure on hillslopes as landslides become more common (e.g. Heimsath *et al.*, 2012). In the SGM, modal slopes of 36° to 38° appear to be controlled by the angle-of-repose wedges of loose debris upslope of rocky outcrops, which we observed in the field (and from the 1 m DEM) to have a similar range in slope. Thus, as hillslopes become rockier, mean slopes increase, and slope distributions become skewed increasingly towards higher slopes while the prevalence of loose debris holds modal slopes to values near the angle of repose (Figure 5a). The topographic signature of this transition from creep to failure emerges most clearly in 1 m data, where the onset of rocky hillslopes can be discerned clearly (Figure 5c). As highlighted by Figure 4b and the Supporting Information, slope distributions derived from 10 m resolution USGS data fail to reproduce important details present in steep catchments, and reinforce the importance of capturing fine scale texture for topographic analysis in mountainous topography.

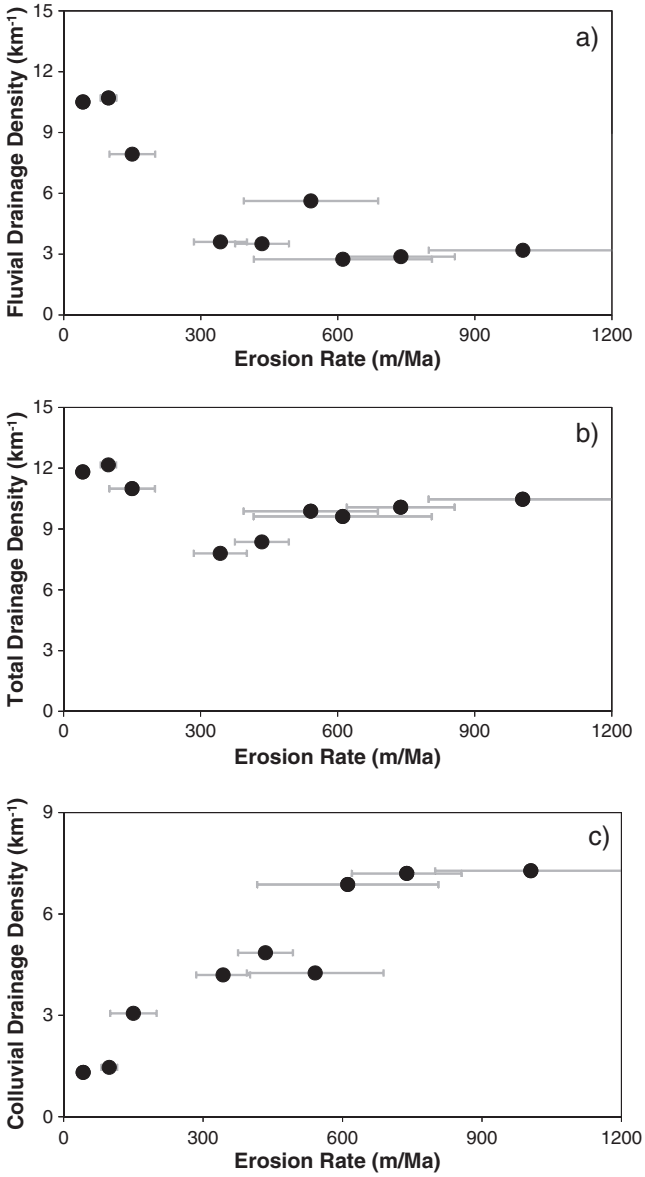

Figure 9. Plots of drainage density against erosion rate for nine catchments shown in Figure 8. Fluvial drainage density (a) is defined by channels following Flint's law scaling in slope-area space. Total drainage density (b) is determined from hand-picked channel heads in areas with rapid increase in contributing area (Figure 7). Colluvial drainage density (c) is calculated as the difference between total and fluvial drainage density.

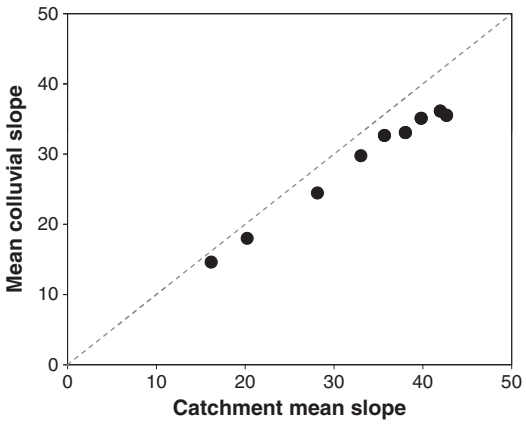

Figure 10. Mean colluvial slope plotted against catchment-mean slope for the nine study catchments shown in Figure 8. Dashed line indicates 1:1 relationship. Colluvial slope is calculated as the slope of a linear fit to each colluvial channel, and the mean colluvial slope is the average of all such channels for each catchment, weighted by channel length.

Why then does mean slope become insensitive to long-term erosion rate, as shown in many studies (Burbank *et al.*, 1996; Montgomery and Brandon, 2002; Binnie *et al.*, 2007; Ouimet *et al.*, 2009; Stock *et al.*, 2009; DiBiase *et al.*, 2010; Norton *et al.*, 2010)? For example, using 10 m resolution topography, DiBiase *et al.* (2010) argued that in the SGM, hillslopes fail to record changes in erosion rate above rates of ~300 m/Ma. Figure 6a suggests, however, that using 1 m LiDAR topography reveals a positive relationship between mean slope and erosion rate for 'threshold' catchments. As mentioned earlier, this positive relationship is likely due to the selection of small, homogeneous study catchments of similar size in the current analysis – there is a strong linear relationship between mean slope as measured with the LiDAR DEM and USGS 10 m DEM ($R^2 = 0{\cdot}99$ for catchments shown in Figure 4). Thus although using higher resolution topographic data enables more precise measurements of hillslope angle, catchment mean slope depends primarily on the hillslope relief structure, and does not change significantly with measurement scale for grid scales much smaller than the typical hillslope length (as opposed to local measurements of slope and curvature). However, the robust inter-relations among topographic

characteristics for the small catchments studied here strongly suggest that the positive relationship between mean slope and erosion rate is not an artifact of site selection bias. In contrast to typical assumptions about threshold hillslopes (e.g. Burbank and Anderson, 2001), hillslopes in the SGM show systematic variation in morphology and texture with increasing mean slope across the full range of relief and erosion rates (Figure 7). Gabet *et al*. (2004) and Korup (2008) suggest that local variations in climate and/or rock strength control slope, rock exposure, and the surface expression of steep hillslopes. That is, as slopes steepen to the point where landsliding begins and rock becomes exposed, differences in meso-scale rock strength control the topographic expression of hillslopes, and decouple hillslope morphology from tectonic processes. While spatial variability in rock strength and local climate probably contribute to the significant scatter in the relationship between erosion rate and both REI and mean slope (Figure 6), the strong inter-relationships observed between mean slope, rock exposure, and slope distributions demonstrate that steepland hillslopes are more sensitive to tectonic processes than previously thought.

One of the key linkages in the study of the climatic, tectonic, and geomorphic evolution of mountain ranges is the relationship between landscape relief and erosion rate. Total landscape relief for unglaciated terrain can be split into its components consisting of fluvial, colluvial, and hillslope relief (Whipple *et al*., 1999; DiBiase *et al*., 2010). While the fluvial network occupies only a small fraction of the areal extent of a typical mountainous landscape, it can account for more than 80% of the total relief structure – an observation that motivates much research into the details of bedrock river incision, and lies behind the strength of the channel steepness index as a topographic metric of erosion rate (Ouimet *et al*., 2009; DiBiase *et al*., 2010). However, Figure 8 implies that the relative contributions to total landscape relief vary with erosion rate as fluvial drainage density decreases. Hillslope relief can be quantified by multiplying mean hillslope length (estimated as one half the inverse of total drainage density and approximately constant in the SGM) by the tangent of mean hillslope angle. Colluvial relief can be determined in a similar fashion using mean colluvial channel slope, hillslope length, and fluvial drainage density, and increases steadily with erosion rate because both the length and slope of colluvial channels increase with erosion rate (Figures 9b and 10). Lague and Davy (2003) note a similar increase in colluvial slopes with erosion rate in the Siwalik Hills of Nepal, and Stock and Dietrich (2003) note that a significant fraction of catchment relief in the Oregon Coast Range is occupied by colluvial channels. It appears then that partitioning relief into its individual process components becomes important for characterizing landscape response to external forcing. However, in the SGM, the total of hillslope and colluvial relief does not exceed 150 m, while local relief measured over a 5 km diameter window can be 1000 m or greater. Although Stock and Dietrich (2003, 2006) have argued that debris flows influence channel slope down to a channel gradient of ~10% (implying a greater fraction of relief in channels influenced by debris-flow scour), we find that all channel segments below the colluvial–fluvial transition as defined here (Figure 7b, Supporting Information) show a consistent relationship between channel steepness and erosion rate (Wobus *et al*., 2006; DiBiase *et al*., 2010). Moreover, DiBiase *et al*. (2010) find a strong linear correlation between channel steepness and 5 km local relief in the SGM. Thus, while threshold hillslopes and colluvial channel networks encode tectonic information in their texture, extent, and slopes, it is the fluvial network (defined as the extent of channels reasonably well described by Flint's law slope-area scaling) that governs kilometer scale relief in steep landscapes.

Conclusion

Our results suggest that high-resolution LiDAR topography reveals complexity and textural details in threshold hillslopes not evident from coarser elevation data. We use detailed panoramic photographs to calibrate a rock exposure index (REI) based on a slope map derived from a 1 m LiDAR-derived DEM. We find that the fraction of slopes greater than 45° closely matches mapped bedrock exposure. While this index likely requires recalibration for use in other landscapes, it highlights the potential for using increasingly available LiDAR datasets to map the distribution of soil and bedrock at a previously unattainable scale. While previous studies suggest that hillslopes fail to record tectonic information in steep landscapes, we show strongly correlated, systematic variations in rock exposure, mean slope, catchment slope skewness, and colluvial and fluvial drainage density as catchment averaged erosion rates increase from about 40 to about 1000 m/Ma. We find two distinct trends in hillslope gradient distributions. For mean slopes less than 30°, little rock is exposed, modal slopes track with mean slopes, and catchment slope skewness decreases with increasing mean slope. For mean slopes greater than 30°, rock exposure increases with mean slope, and the prevalence of angle-of-repose debris slopes holds modal slopes at about 37°. As a result, skewness increases as mean slopes steepen up to 45°, which cannot be discerned in similar analysis of 10 m USGS topographic data. Our detailed analysis of the extent of the fluvial and colluvial channel network reveals that colluvial drainage density increases with average erosion rate at the expense of the fluvial network. This keeps total drainage density roughly constant and highlights the need for better quantifying the role of debris flow processes in threshold landscapes.

Acknowledgments—This work was supported by funding from the Geomorphology and Land Use Dynamics Program at NSF (EAR-0518998 to AMH, EAR-0724194 to KXW). Laser altimetry was acquired and processed by the National Center for Airborne Laser Mapping (NCALM) with support from Arizona State University (AMH, KXW), Caltech (Michael Lamb), and the USGS. Taufique Mahmood helped develop the Rock Exposure Index. Comments by Dimitri Lague and an anonymous reviewer helped improve the manuscript.

Supporting Information

Supporting information may be found in the online version of this article.

References

Binnie SA, Phillips WM, Summerfield MA, Fifield LK. 2007. Tectonic uplift, threshold hillslopes, and denudation rates in a developing mountain range. *Geology* **35**: 743–746. DOI. 10.1130/g23641a.1

Burbank DW, Anderson RS. 2001. Tectonic Geomorphology. Blackwell: Malden, MA.

Burbank DW, Leland J, Fielding E, Anderson RS, Brozovic N, Reid MR, Duncan C. 1996. Bedrock incision, rock uplift and threshold hillslopes in the northwestern Himalayas. *Nature* **379**: 505–510. DOI. 10.1038/379505a0

Carson MA, Petley DJ. 1970. The existence of threshold hillslopes in the denudation of the landscape. *Transactions of the Institute of British Geographers* **49**: 71–95. DOI. 10.2307/621642

DiBiase RA, Whipple KX, Heimsath AM, Ouimet WB. 2010. Landscape form and millennial erosion rates in the San Gabriel Mountains, CA. *Earth and Planetary Science Letters* **289**: 134–144. DOI. 10.1016/j.epsl.2009.10.036

Dunai TJ. 2000. Scaling factors for production rates of in situ produced cosmogenic nuclides: a critical reevaluation. *Earth and Planetary Science Letters* **176**: 157–169. DOI. 10.1016/s0012-821x(99)00310-6

Gabet EJ, Pratt-Sitaula BA, Burbank DW. 2004. Climatic controls on hillslope angle and relief in the Himalayas. *Geology* **32**: 629–632. DOI. 10.1130/g20641.1

Heimsath AM, DiBiase RA, Whipple KX. 2012. Soil production limits and the transition to bedrock dominated landscapes. *Nature Geoscience*. DOI: 10.1038/NGEO1380

Heimsath AM, Dietrich WE, Nishiizumi K, Finkel RC. 1997. The soil production function and landscape equilibrium. *Nature* **388**: 358–361. DOI. 10.1038/41056

Heimsath AM, Furbish DJ, Dietrich WE. 2005. The illusion of diffusion: field evidence for depth-dependent sediment transport. *Geology* **33**: 949–952. DOI. 10.1130/g21868.1

Hilley GE, Arrowsmith JR. 2008. Geomorphic response to uplift along the Dragon's Back pressure ridge, Carrizo Plain, California. *Geology* **36**: 367–370. DOI. 10.1130/g24517a.1

Howard AD. 1997. Badland morphology and evolution: interpretation using a simulation model. *Earth Surface Processes and Landforms* **22**: 211–227.

Korup O. 2008. Rock type leaves topographic signature in landslide-dominated mountain ranges. *Geophysical Research Letters* **35**: L11402. DOI. 10.1029/2008gl034157

Lague D, Davy P. 2003. Constraints on the long-term colluvial erosion law by analyzing slope-area relationships at various tectonic uplift rates in the Siwaliks Hills (Nepal). *Journal of Geophysical Research* **108**: 2129. DOI. 10.1029/2002jb001893

Lavé J, Burbank D. 2004. Denudation processes and rates in the Transverse Ranges, southern California: erosional response of a transitional landscape to external and anthropogenic forcing. *Journal of Geophysical Research* **109**: F01006. DOI. 10.1029/2003jf000023

Montgomery DR. 2001. Slope distributions, threshold hillslopes, and steady-state topography. *American Journal of Science* **301**: 432–454. DOI. 10.2475/ajs.301.4-5.432

Montgomery DR, Brandon MT. 2002. Topographic controls on erosion rates in tectonically active mountain ranges. *Earth and Planetary Science Letters* **201**: 481–489. DOI. 10.1016/s0012-821x(02)00725-2

Montgomery DR, Dietrich WE. 1988. Where do channels begin? *Nature* **336**: 232–234. DOI. 10.1038/336232a0

Montgomery DR, Dietrich WE. 1989. Source areas, drainage density, and channel initiation. *Water Resources Research* **25**: 1907–1918. DOI. 10.1029/WR025i008p01907

Montgomery DR, Foufoula-Georgiou E. 1993. Channel network source representation using digital elevation models. *Water Resources Research* **29**: 3925–3934. DOI. 10.1029/93wr02463

National Research Council. 2010. Landscapes on the Edge: New Horizons for Research on Earth's Surface. National Academies Press: Washington, DC.

Norton KP, von Blanckenburg F, Kubik PW. 2010. Cosmogenic nuclide-derived rates of diffusive and episodic erosion in the glacially sculpted upper Rhone Valley, Swiss Alps. *Earth Surface Processes and Landforms* **35**: 651–662. DOI. 10.1002/esp.1961

Ouimet WB, Whipple KX, Granger DE. 2009. Beyond threshold hillslopes: channel adjustment to base-level fall in tectonically active mountain ranges. *Geology* **37**: 579–582. DOI. 10.1130/g30013a.1

Passalacqua P, Do Trung T, Foufoula-Georgiou E, Sapiro G, Dietrich WE. 2010a. A geometric framework for channel network extraction from lidar: nonlinear diffusion and geodesic paths. *Journal of Geophysical Research-Earth Surface* **115**: F01002. DOI. 10.1029/2009jf001254

Passalacqua P, Tarolli P, Foufoula-Georgiou E. 2010b. Testing space-scale methodologies for automatic geomorphic feature extraction from lidar in a complex mountainous landscape. *Water Resources Research* **46**: W11535. DOI. 10.1029/2009wr008812

Peterson MD, Wesnousky SG. 1994. Fault slip rates and earthquake histories for active faults in southern California. *Bulletin of the Seismological Society of America* **84**: 1608–1649.

Reneau SI, Dietrich WE, Donahue DJ, Jull AJT, Rubin M. 1990. Late Quaternary history of colluvial deposition and erosion in hollows, Central California Coast Ranges. *Geological Society of America Bulletin* **102**: 969–982.

Roering JJ. 2008. How well can hillslope evolution models "explain" topography? Simulating soil transport and production with high-resolution topographic data. *Geological Society of America Bulletin* **120**: 1248–1262. DOI. 10.1130/b26283.1

Roering JJ, Kirchner JW, Dietrich WE. 1999. Evidence for nonlinear, diffusive sediment transport on hillslopes and implications for landscape morphology. *Water Resources Research* **35**: 853–870. DOI. 10.1029/1998wr900090

Roering JJ, Perron JT, Kirchner JW. 2007. Functional relationships between denudation and hillslope fonn and relief. *Earth and Planetary Science Letters* **264**: 245–258. DOI. 10.1016/j.epsl.2007.09.035

Schmidt KM, Montgomery DR. 1995. Limits to relief. *Science* **270**: 617–620. DOI. 10.1126/science.270.5236.617

Schorghofer N, Rothman DH. 2002. Acausal relations between topographic slope and drainage area. *Geophysical Research Letters* **29**: 1633. DOI. 10.1029/2002gl015144

Spotila JA, House MA, Blythe AE, Niemi NA, Bank GC. 2002. Controls on the erosion and geomorphic evolution of the San Bernardino and San Gabriel Mountains, southern California. *Geological Society of America Special Paper* **365**: 205–230.

Stock J, Dietrich WE. 2003. Valley incision by debris flows: evidence of a topographic signature. *Water Resources Research* **39**: 1089. DOI. 10.1029/2001wr001057

Stock J, Dietrich WE. 2006. Erosion of steepland valleys by debris flows. *Geological Society of America Bulletin* **118**: 1125–1148. DOI. 10.1130/b25902.1

Stock GM, Frankel KL, Ehlers TA, Schaller M, Briggs SM, Finkel RC. 2009. Spatial and temporal variations in denudation of the Wasatch Mountains, Utah, USA. *Lithosphere* **1**: 34–40. DOI. 10.1130/l15.1

Strahler AN. 1950. Equilibrium theory of erosional slopes approached by frequency distribution analysis. *American Journal of Science* **248**: 673–696.

Tarboton DG. 1997. A new method for the determination of flow directions and upslope areas in grid digital elevation models. *Water Resources Research* **33**: 309–319. DOI. 10.1029/96wr03137

Tarboton DG, Bras RL, Rodriguezituibe I. 1992. A physical basis for drainage density. *Geomorphology* **5**: 59–76. DOI. 10.1016/0169-555x(92)90058-v

Tucker GE, Bras RL. 1998. Hillslope processes, drainage density, and landscape morphology. *Water Resources Research* **34**: 2751–2764. DOI. 10.1029/98wr01474

Tucker GE, Hancock GR. 2010. Modelling landscape evolution. *Earth Surface Processes and Landforms* **35**: 28–50. DOI. 10.1002/esp.1952

Whipple KX, Tucker GE. 1999. Dynamics of the stream-power river incision model: implications for height limits of mountain ranges, landscape response timescales, and research needs. *Journal of Geophysical Research* **104**: 17661–17674. DOI. 10.1029/1999jb900120

Whipple KX, Kirby E, Brocklehurst SH. 1999. Geomorphic limits to climate-induced increases in topographic relief. *Nature* **401**: 39–43. DOI. 10.1038/43375

Wobus C, Whipple KX, Kirby E, Snyder N, Johnson J, Spyropolou K, Crosby B, Sheehan D. 2006. Tectonics from topography: procedures, promise, and pitfalls. *Geological Society of America Special Paper* **398**: 55–74.

Wolinsky MA, Pratson LF. 2005. Constraints on landscape evolution from slope histograms. *Geology* **33**: 477–480. DOI. 10.1130/g21296.1